Aeolian dust dispersal patterns since the last glacial period in eastern Central Asia: Insights from a loess-paleosol sequence in the Ili Basin

Yue Li[1,2,3], Yougui Song[1]*, Kathryn E. Fitzsimmons[2], Hong Chang[1], Rustam Orozbaev[4,5], Xinxin Li [1,2]

1 State Key Laboratory of Loess and Quaternary Geology, Institute of Earth Environment, Chinese Academy of Sciences, Xi'an, 710061, China

2 Research Group for Terrestrial Palaeoclimates, Max Planck Institute for Chemistry, Mainz, 55128, Germany

3 College of Earth Science, University of Chinese Academy of Sciences, Beijing, 100049, China

4 Research Center for Ecology and Environment of Central Asia, Chinese Academy of Sciences, Urumqi, 830011, China

5 Institute of Geology, National Academy of Sciences, Bishkek, 720040, Kyrgyzstan

* Corresponding author:

Dr. Yougui Song

E-mail: syg@ieecas.cn

State Key Laboratory of Loess and Quaternary Geology

Institute of Earth Environment, Chinese Academy of Sciences

No. 97 Yanxiang Road, Yanta, Xi'an 710061, China

Tel. 86-29 6233 6216

Fax. 86-29 6233 6216

Abstract

The extensive loess deposits of the Eurasian mid-latitudes provide important terrestrial archives of Quaternary climatic change. As yet, however, loess records in Central Asia are poorly understood. Here we investigate the grain size and magnetic characteristics of loess from the Nilka (NLK) section in the Ili Basin of eastern Central Asia. Weak pedogenesis suggested by frequency-dependent magnetic susceptibility (χ_{fd}%) and magnetic susceptibility (MS) peaks in primary loess suggest that MS is more strongly influenced by allogenetic magnetic minerals than pedogenesis, and may therefore be used to indicate wind strength. This is supported by the close correlation between variations in MS and proportions of the sand-sized fraction. To further explore the temporal variability in dust transport patterns, we identified three grain size end members (EM1, mode size 47.5 μm; EM2, 33.6 μm; EM3, 18.9 μm) which represent distinct aerodynamic environments. EM1 and EM2 are inferred to represent grain-size fractions transported from proximal sources in short-term, near-surface suspension during dust outbreaks. EM3 appears to represent a continuous background dust fraction under non-dust storm conditions. Of the three end members, EM1 is most likely the most sensitive recorder of wind strength. We compare our EM1 proportions and mean grain size from NLK with the Jingyuan section in the Chinese loess plateau, and assess these in the context of modern and Holocene climate data, and suggest that the Siberian high-pressure system is the dominant influence on wind dynamics and thus loess deposition in the eastern Ili Basin. Six millennial-scale cooling (Heinrich) events can be identified in the NLK loess records. Our grain-size data support the hypothesis that the Siberian High acts as teleconnection between the climatic systems of the North Atlantic and East Asia in the high northern latitudes, but not for the mid-latitude westerlies.

Key words: Last glacial, Ili Basin, Central Asia, loess, magnetic susceptibility, grain size, paleoclimate

1 Introduction

Central Eurasia experiences extremely continental climatic conditions, in large part due to its position far from the oceans. Arid Central Asia (ACA), the mid-latitude region spanning the Caspian Sea across to the eastern Tien Shan mountains, is therefore a sensitive recorder of past climate change due to its location in the transitional region between the Asian monsoons (Dettman et al., 2001;Cheng et al., 2012), mid-latitude westerlies (Vandenberghe et al., 2006) and North Asian polar front (Machalett et al., 2008). The relative importance and intensity of these major climate subsystems has varied across the latitudinal and longitudinal range of Central Asia through time. Thus identification of the predominant climate regimes in this region, using geological archives, is a crucial precondition for tracing paleoclimatic evolution.

One of the most promising potential palaeoenvironmental archives in ACA is its widespread, thick loess deposits. Loess is one of the most important archives of Quaternary climate change (Maher, 2016;Muhs, 2013). In Central Asia, the loess deposits drape the piedmont slopes of the major mountain ranges - the Tian Shan, Alai, Altai and Pamirs - from Xinjiang province in China through Kazakhstan, Kyrgyzstan and Uzbekistan, into Tajikistan. While recent years have witnessed increasing loess-based datasets in the region (Dodonov et al., 2006;Feng et al., 2011;Li et al., 2016c;Li et al., 2016b;Machalett et al., 2006;Smalley et al., 2006;Song et al., 2014;Song et al., 2015;Song et al., 2012;Yang et al., 2006;Youn et al., 2014;Fitzsimmons et al., 2016), the forcing

mechanisms and the climatic conditions responsible for loess-paleosol sequences formation are as yet not systematically understood (Fitzsimmons et al., 2016;Machalett et al., 2008;Li et al., 2016a;Song et al., 2017b).

Evidence for millennial-scale climatic oscillations associated with the Greenland (*Dansgaard/Oeschger (D-O) events*) (Dansgaard et al., 1993) and cool phases associated with iceberg calving into the North Atlantic (*Heinrich (H) events*) (Bond et al., 1992) have been found in the form of grain-size variations in loess deposits in Chinese Loess Plateau (CLP) (Sun et al., 2012;Porter and An, 1995;Chen et al., 1997b) and Europe (Antoine et al., 2009;Rousseau et al., 2007;Zeeden et al., 2016). Data for Central Asian loess do not as yet exist at this resolution (Li et al., 2016b;Song et al., 2017a), despite its strategic location as a likely environmental bridge between the North Atlantic and East Asian Monsoon climatic regions.

The Ili Basin of Central Asia hosts thick loess deposits in the strategic central eastern part of ACA (Song et al., 2014). The basin is surrounded to the south and north by the Tian Shan mountain range, widens to the west and drains into endorheic Lake Balkhash (Fig. 1), and provides a conducive situation for loess accumulation. In this paper we present new data on the physical properties of a 20.4 m thick loess deposit at Nilka (NLK) in the eastern Ili Basin. We investigate variations in grain size distributions and magnetic properties in order to investigate likely links with environmental dynamics.

2 Physical geography

The Ili Basin (78° ~ 85° E and 42° 30′ ~ 44° 30′ N) straddles southeast Kazakhstan and northwest China. It is an intermontane basin opening westward towards the Ili drains into Lake Balkhash which is in the semi-arid transitional region between the steppe and full deserts of Central Asia. The Northern and Southern Tian Shan form the northern and southern margins of the basin (Fig. 1a).

This region has a semi-arid, continental climate, with a strong precipitation gradient dependent on altitude. The altitude of the basin floor is 500 ~ 780 m; the northern Tian Shan Range reaches altitudes of > 4000 m a.s.l. and the southern Tian Shan mountains range between 3000 ~7000 m a.s.l. towards the catchment divide. Mean annual precipitation (MAP) ranges between 200-500 mm on the plains, and mean annual temperature (MAT) ranges from 2.6-10.4°C (Li, 1991;Ye, 1999). The surface vegetation in this region is dominated by *Desert Steppe* and *Steppe* and the zonal soils comprise *Sierozem*, *Castonozem* and *Chernozem*.

Modern meteorological data (2009 – 2013) show a MAP of 354 mm and a MAT of 7.3°C in Nilka site (data from the China Meteorological Data Network: http://data.cma.cn/).

Fig. 1 The location of study area and the photo of Nilka (NLK) section.

3 Materials and methods

3.1 Section and sampling

The Nilka (NLK) section (83.25°E, 43.76°N, 1253 m a.s.l) is situated on the second terrace of the right bank of the Kashi River, a tributary of the Ili River. The site is located in the eastern Ili Basin of far western China, adjoining the Northern Tian Shan to the north (Fig. 1b). The section has a thickness of 20.4 m and overlies fluvial sands and gravels (Fig.1c). The profile has been exposed by local residents for making bricks, and recently formed the focus of a geochronological study comparing luminescence with radiocarbon methods (Song et al., 2015). According to the dating

results, the NLK loess started to accumulate since ~ 70 ka. Stratigraphically and geochronologically, the loess package at NLK is equivalent to the L1 loess unit (also known as Malan loess) and S0 paleosol unit (known as Holocene Heilu soil) in the CLP (Liu, 1985a). Although largely homogeneous in appearance, two weak paleosols (at 5.0 – 7.0 m and 15.7 – 18.0 m depths) were identified in the section by field observations. We therefore divided the NLK stratigraphy into S0, L1L1, L1S1, L1L2, L1S2 and L1L3 units (Fig. 1c).

After cleaning the NLK section to remove dry, weathered sediment, samples were collected at intervals of 2 cm. A total of 1026 bulk samples were prepared for measurements of physical characteristics. Because the optically stimulated luminescence (OSL) dating is more reliable for constructing a loess chronology than bulk sediment AMS ^{14}C dates (Song et al., 2015), this study uses the previously published OSL dating results as the basis for our age model.

3.2 Grain-size analyses

Prior to grain size measurements, 0.5 g of dry bulk sample was pretreated by the removal of organic matter and carbonate using H_2O_2 and HCl, respectively (Lu and An, 1997). Samples were then dispersed in an ultrasonic bath for 5 min with 10 ml 10% $(NaPO_3)_6$ solution. Grain size distribution was analyzed using a Malvern 2000 laser instrument at the State Key Laboratory of Loess and Quaternary Geology, Institute of Earth Environment, Chinese Academy of Sciences. Particle size distribution was calculated for 100 grain size classes within a measuring range of 0.02−2000 μm. Replicate analyses indicated an analytical error of < 2% for the mean grain size.

End-member unmixing of loess grain-size distributions is based on the hierarchical Bayesian model for end-member modeling analysis (BEMMA; Yu et al. (2016)). Grain-size parameters were calculated from the analytical data with GRADISTAT (Version 4.0; Blott (2000)).

Two samples (NLK1106 at 11.06 m and NLK1840 at 17.8 m) were also selected for the extraction and measurement of mineral-specific quartz grain size according to published methods (Sun et al., 2000a). The isolated quartz grain samples (Fig. S1) were then analyzed by the Malvern 2000 laser instrument so that comparisons of quartz grain and bulk samples could be performed to investigate the weathering degree of NLK loess.

3.3 Magnetic susceptibility measurements

Magnetic susceptibility was measured with a Bartington MS2 meter at the State Key laboratory of Loess and Quaternary Geology, Institute of Earth Environment, Chinese Academy of Sciences. Samples were oven-dried at 40°C for 24 hours. Subsamples of 10 g from each sample were then precisely weighed for magnetic measurements. Low- (0.47 kHz) and high- (4.7 kHz) frequency magnetic susceptibility (χ_{lf} and χ_{hf}, respectively) were measured. The absolute frequency-dependent magnetic susceptibility was calculated as $\chi_{fd} = \chi_{lf} - \chi_{hf.}$ Frequency-dependent magnetic susceptibility was defined and calculated as $\chi_{fd}\ \% = [(\chi_{lf} - \chi_{hf})/ \chi_{lf}] \times 100\%$.

4 Results

4.1 Magnetic susceptibility variations

Both magnetic susceptibility (MS) data and stratigraphy show a close correspondence throughout the NLK section. We observe higher MS values within primary loess and lower values within paleosols. The exception to this trend is the modern (S0) soil which yields high MS values (Fig. 2).

Fig. 2 Lithology and magnetic susceptibility characteristics (χ_{lf}, χ_{fd} and χ_{fd}%) of the NLK section.

The χ_{lf} values of the S0 unit are higher than for the L1 unit, with an average of 98.13 × $10^{-8}m^3kg^{-1}$. The χ_{lf} values of the L1L1 unit vary from 56.5 − 103.9 × $10^{-8}m^3kg^{-1}$, decreasing down-profile. The χ_{lf} value abruptly decreases at c. 5 m, with generally lower values in the L1S1 unit, averaging 62.58 × $10^{-8}m^3kg^{-1}$. χ_{lf} in the L1L2 unit gradually increases down profile, with significant fluctuations in the lower part; χ_{lf} values vary from 67 − 102.55 × $10^{-8}m^3kg^{-1}$. Lower χ_{lf} values are observed in L1S1 unit with an average value of 57.99 × $10^{-8}m^3kg^{-1}$. In the L1L3 unit, the χ_{lf} values vary with greater amplitude around an average value of 68.74 × $10^{-8}m^3kg^{-1}$.

Absolute frequency-dependent magnetic susceptibility (χ_{fd}) values likewise vary with stratigraphy. The S0 unit yields the highest χ_{fd} value. The L1 unit is characterized by relatively consistent and lower χ_{fd} values. Frequency-dependent magnetic susceptibility (χ_{fd}%) yields the same trend as χ_{fd}, although χ_{fd}% values clearly increase in the central part of L1S2.

4.2 Mixing model of loess grain-size distributions

The mean grain-size distribution, and variation range of volume frequencies for each grain-size class in the dataset, are presented in Fig. 3a. The overall grain-size frequency curve shows a unimodal pattern, slightly skewed towards the coarser side, with the primary mode ranging from 11.9 – 47.5 µm. An additional small grain size peak occurs at c. 0.4 – 2 µm. Three unmixed end members were identified (Fig. S2), yielding fine-skewed grain-size distributions with clearly defined modes of 47.5 µm (EM1), 33.6 µm (EM2) and 18.9 µm (EM3) (Fig. 3b).

Fig. 3 End-member modelling results of the grain-size dataset of the NLK section. (a) Mean size distribution and range of volume frequency for each size class. (b) Modelled end-members according to the three-end-member model (modal sizes: ~ 47.5 µm, ~ 33.6 µm and ~ 18.9 µm). Size limits of clay, silt and sand fractions determined by laser particle sizer differ from those derived by the pipette method. The upper limits of grain-size classes used here are at 4.6/5.5 µm for clay, 26 µm for fine silt, and 52 µm for coarse silt, as previously published by Konert and Vandenberghe (1997). Sand is designated for particle sizes > 52 µm. Therefore, EM1 and EM2 correspond to coarse silt and EM3 to fine silt.

The proportional distribution of the end members down the section is shown in Fig. 4. In the primary loess units (L1L1, L1L2 and L1L3), the deposits are dominated by the coarser silt EM1 and EM2, while higher proportions of fine silt EM3 are observed within the soil horizons (S0, L1S1 and L1S2). EM1 displays high frequency, large amplitude fluctuations down the profile, varying between 0.09 – 0.72, and clearly dominates the primary loess units and occurs in low proportions in the soil units (Fig. 4). EM2 shows a similar trend to EM1, but with less variability down profile. Proportions of EM2 range between 0.11 − 0.66 with minimal fluctuations within individual units, and proportions decrease significantly in the soil units S0 and L1S2. Proportions of EM3 remain consistently low within the primary loess units, and increase to 0.46 and 0.8 within the soil horizons S0 and L1S2 respectively.

Fig. 4 Proportional contributions of the three end-members in the NLK section.

5 Discussion

5.1 Impacts of wind strength on magnetic susceptibility variations

Magnetic susceptibility (MS) in loess is predominantly determined by the concentration of

iron-bearing magnetic minerals within the sediment (Liu et al., 1999;Liu et al., 1994;Song et al., 2010). Generally, this varies between primary loess and soil horizons. Soils generally experience an enrichment in magnetic minerals (higher MS), compared with primary loess (Zhou et al., 1990;Maher and Thompson, 1992;Heller and Evans, 1995;Heller and Liu, 1984;Ding et al., 2002;Buggle et al., 2009).

The contrast between high and low MS in paleosols and primary loess, respectively, typically forms the basis for the stratigraphic differentiation of loess deposits. The main MS variations in the NLK loess sequence, with the exception of the S0 unit, however, do not follow this trend (Fig. 2). At NLK, lower MS values are found in the paleosols and higher MS in loess units. A similar case also occurs in the L1 loess layers at other sites in the Ili Valley, such as the TLD, ZKT and AXK sections (Fig. 1) (Jia et al., 2010;Jia et al., 2012;Song et al., 2010).

χ_{fd} indicates the concentration of magnetic particles within a small grain size range across the superparamagnetic (SP)/stable single domain (SSD) boundary (Liu et al., 2012) (magnetite, < ~100 nm; maghemite, < ~20 μm). Particles with this grain size are considered to form *in situ* within soils during pedogenesis (Maher and Taylor, 1988;Zhou et al., 1990). Therefore, χ_{fd} can serve as a direct proxy for pedogenesis (Heller et al., 1993;Maher and Thompson, 1995;Liu et al., 2007;Buggle et al., 2014). In the NLK section, χ_{fd} yields consistently low values throughout the sequence and indicates no clear enrichment even in the paleosol layers L1S1 and L1S2. Comparison between χ_{lf} vs. χ_{fd} down profile shows no correlation between MS and SP particles (Fig, S3c). These results suggest that SP particles played only a minor role in MS enhancement in the NLK loess.

χ_{fd}% is used as a proxy to determine the contribution of SP particles to MS (Zhou et al., 1990;Liu et al., 1992). At NLK section, however, we also observe consistently low χ_{fd}% values in both loess and paleosol layers, with a slight increase only in the L1S1 paleosol. This observation reinforces our interpretation that the content of SP particles is very low, and consequently that their contribution to MS can be ignored.

The low proportions of SP particles in the NLK loess imply that the pseudo-single-domain (PSD) and multi-domain (MD) magnetic grains, rather than SP grains forming in situ, are more influential for the magnetic enhancement at this site. Since PSD and MD magnetic minerals are difficult to produce during pedogenesis (Song et al., 2010), such minerals are more likely to be detrital in nature, deriving from the original protolith.

Fig. 5 Comparison of different grain size fractions of NLK loess with χ_{lf} (limits of grain-size classes after Konert and Vandenberghe (1997)).

In some cases, moist conditions associated with pedogenesis may result in the weathering and dissolution of the magnetic minerals maghemite and magnetite (Nawrocki et al., 1996;Maher, 1998;Grimley and Arruda, 2007). In such cases, a negative relationship between magnetic susceptibility and pedogenesis can develop, in contrast to the classical situation whereby χ_{fd} is enhanced. At NLK section, however, we observe no textures caused by groundwater fluctuations. We therefore exclude groundwater fluctuations and high levels of precipitation as a factor in our MS characteristics at NLK section.

In the wind velocity/vigor model (also known as the Alaskan or Siberian model), wind strength affects MS values of loess through the physical sorting of magnetic grains (Beget and Hawkins, 1989). The influence of this process on MS values in loess can be assessed by investigating the

correlation between MS and coarser (silt or sand) and finer clay percentages (Fig. S3). At NLK, low MS values in the S0 soil between 0 – 0.5 m correlate positively with clay percentage variations (Fig. S3a), while higher MS values at depths greater than > 0.5 m correlate closely with increased sand concentrations (Fig. S3b). We therefore propose that MS enhancement at NLK is likely driven by wind strength. Under this scenario, weak pedogenesis prevented the efficient production of SP grains (Fig. 2), and allogenetic magnetic minerals associated with dust transportation made a greater contribution to the MS. Wind strength can therefore be interpreted as the main influence on MS variations at NLK. The enhancement of magnetic susceptibility in NLK loess most likely falls into region A in Fig. 9 of Liu et al. (2013). Region A represents the area where the climate is arid, and pedogenesis is weak and dominated by physical weathering (Liu et al., 2013). Therefore, we can use the "wind theory" to decipher the MS variations of NLK loess. Weak pedogenesis enables preservation of primary atmospheric dust contributions to NLK.

5.2 Genetic interpretations of end members in loess grain size

Grain-size analysis was conducted in order to understand wind dynamics (strength and direction) during loess deposition (Liu, 1985b;Lu and An, 1998;Sun et al., 2010). Grain-size analysis provides information on sediment depositional mechanisms as well as an insight into spatio-temporal changes in deposition, provided factors such as vegetation, pedogenesis, grain size of source sediments, and distance from the deposition area to source area are taken into account (Qin et al., 2005;DiPietro et al., 2017;Obreht et al., 2015;Terhorst et al., 2012;Ding et al., 2005;Ding et al., 1999;Yang and Ding, 2008).

Statistical analysis of loess grain-size offers new opportunities for understanding paleoclimate variations. Studies increasingly use grain-size partitioning to identify sub-populations within bulk samples. There are two dominant approaches to unmixing grain-size spectra: parametric decomposition (e.g. Sun et al., 2002) and non-parametric decomposition (e.g. Prins and Vriend, 2007;Weltje, 1997; Weltje and Prins, 2007) . Based on the statistical datasets generated, the different end members can be interpreted to infer distinct atmospheric transport mechanisms, modes and travel distances (Ujvari et al., 2016). In some cases, the end-member approach has been used to identify variation in the geological context or source area (Prins et al., 2007). We investigated the applicability of this approach to the Ili Basin loess at NLK by unmixing grain-size distributions with BEMMA (Yu et al., 2016), generating a mixing model consisting of three end members (Fig. S2).

Relying largely on samples from the Eurasian loess belt extending from the Russian Plain north of the Caspian Sea eastwards to the Tibetan Plateau and CLP, Vandenberghe (2013) applied the visual inspection of grain-size distribution curves and EMMA end-member analysis to define the characteristic grain-size distribution of primary loess deposits and interpret the likely conditions of transport and deposition. Using the sediment groups identified in Vandenberghe (2013), some studies interpreted multiple sources for loess sediments (Yang et al., 2016;Nottebaum et al., 2015;Nottebaum et al., 2014). In this study, we apply the end-member analysis of the NLK loess to the sediment groups of Vandenberghe (2013) in an effort to reconstruct dominant aeolian processes.

Fine sand ('*sediment type 1.a*' in Vandenberghe (2013)) is a typical component of loess deposits near to or overlying river terraces. Although the NLK section lies on the second terrace of the Kashi River and therefore close to a potential source of coarser grained material, the fine-sand end member is completely absent. Modal grain sizes in this range (c. 75 μm) are common in loess along the Huang Shui and Yellow Rivers in China (Vriend and Prins, 2005;Vandenberghe et al., 2006;Prins et al., 2009), the Danube and Tisza rivers in Serbia (Bokhorst et al., 2011), and the Mississippi valley

in the USA (Jacobs et al., 2011). Since this fraction is interpreted to originate from proximal sources, the grain size of the available source material, rather than wind energy, plays a more important role in the presence and proportions of this grain size (Vandenberghe, 2013). The lack of fine sand at NLK may be attributed to 1) its location in the upper reaches of the Kashi river (Fig. 1b) in a region which lacks available supplies of fine sand; 2) the V-shaped nature of the channel which is not conducive to aeolian entrainment of bank deposits; and 3) the relatively high altitude of NLK within the basin which inhibits transport and deposition of coarser sediment grains (Vandenberghe, 2013).

The three members identified at NLK correspond to coarse silt (EM1 and EM2) and fine silt (EM3) (Fig. 3b). Each likely represent different kinds of depositional processes which operated throughout the accumulation of the deposit at NLK. Here we focus on the implications of these three end members for understanding past environmental conditions responsible for loess-paleosol sequences formation.

EM1 has a modal grain size of 47.5 μm (Fig. 3b), which approximately corresponds to the '*subgroup 1.b.1*' of Vandenberghe (2013). The mode is similar to end members identified in loess from the CLP and north-eastern Tibetan Plateau (NE-TP) (EM-2: 44 μm) (Vriend et al., 2011). The size of this component is unlikely to be due to longer distance transport. Rather, it is inferred to derive from shorter distance transport of suspended load (Vriend et al., 2011;Vandenberghe, 2013). Coarser particles (>20 μm) rarely reach suspension above the near surface (0 − 200 m above the ground). When entrained by wind, they do not remain in suspension for long enough to travel long distances (Tsoar and Pye, 1987;Pye, 1987). Since the average grain-size of EM1 is 26.74 μm (calculated after Folk and Ward (1957)), we infer that this fraction was transported mainly during short-term suspension episodes at lower elevations by surface winds, and deposited short distances downwind of the source. These short-term suspension episodes may correspond to spring-summer dust storms. Our interpretation is supported by present-day dust measurements on the CLP which identify a similar modal grain-size during such events (Sun et al., 2003).

EM2 represents a mode at 33.6 μm (Fig. 3b). It lies towards the finer end of the range of '*subgroup 1.b.2*' (Vandenberghe, 2013). Comparable loess of the same grain size has been identified in loess from the northern Qilian Shan/Hexi Corridor (EM2: 33 μm) in northern China, which was also interpreted as depositing from short-term suspension (Nottebaum et al., 2015). Loess of this grain size has been attributed to dust fallout (Pye, 1995;Muhs and Bettis, 2003) and fallout from low-altitude suspension clouds (Sun et al., 2003), as measured from modern depositional events. This fraction requires less wind energy than EM1, is transported further, is more widely distributed, and therefore comprises a higher proportion of distal loess populations (Vandenberghe, 2013). We propose that EM2 was transported mainly in short-term, near-surface suspension during dust storms, and that wind strength controlled the relative proportions of EM1 and EM2 through time (see the mirror image relationships over millennial scales in Fig. 4). This interpretation implies that both EM1 and EM2 have the same origin.

The grain-size distribution of EM3 has a modal peak at 18.9 μm (Fig. 3b). This population belongs to '*subgroup 1.c.1*' in Vandenberghe (2013). This population is also widespread in loess from the CLP and NE-TP (Prins et al., 2007;Prins and Vriend, 2007), the Danube Basin loess of Europe (Bokhorst et al., 2011;Varga, 2011). It is particularly common in loess of interglacial age (Vriend, 2007). There is as yet no consensus regarding the transport processes responsible for this grain size population. On the one hand, researchers have suggested that grains of this size can be lifted by strong vertical air movement and subsequently incorporated into the high-level westerly

air streams (Pye, 1995;Pye and Zhou, 1989). This process would link EM3 with long-term suspension transport driven by high-level Westerlies (Prins et al., 2007;Vriend et al., 2011;Nottebaum et al., 2014;Vandenberghe, 2013). Conversely, Zhang et al. (1999) argued that < 20 μm particle fractions derives from "non-dust storm processes" associated with north-westerly surface winds. We argue for the latter on the basis that the EM3 modal grain size from the CLP and NE-TP is coarser (Vriend et al., 2011) than EM3 at NLK in the Ili Valley, which is located further west. If EM3 was transported by high-level westerlies, then one would expect either no significant change (Rea et al., 1985;Rea and Hovan, 1995), or a decrease in grain size from west to east concomitant with wind direction. Furthermore, with mathematical fitting, Sun et al. (2004) related a fine component (2 – 8 μm) to high-altitude westerlies. This fine component is comparable to '*subgroup 1.c.2*' of Vandenberghe (2013) but is not consistent with our modal size of EM3. Observations of modern aeolian processes at the southern margins of the Tarim Basin indicate that fine grain sizes similar to EM3 (8 − 15 μm) are deposited by settling during low velocity wind conditions (Lin et al., 2016). Particle-size distributions of background dust from the northern slopes of the Tianshan Mountains also typically yield a modal peak of approximately 10 μm (Schettler et al., 2014). We therefore infer the EM3 modal peak to derive from low altitude, non-dust storm processes.

Fine particles can also be incorporated into silt- or sand-sized aggregates which can be transported by a range of wind velocities, including dust storms (Qiang et al., 2010;Pye, 1995;Derbyshire et al., 1998;Mason et al., 2003). For example, Ujvari et al. (2016) argued that ~ 1 – 20 μm fractions are affected by aggregation, as shown by comparison between minimally and fully dispersed grain size distribution measurements of loess samples from southern Hungary. Under higher wind velocity conditions, aggregates should co-vary with the coarser EM1 particles transported by surface winds during dust storms. However, since this model is unlikely to hold for EM3 particles (Fig. 4), the aggregate model is unlikely to be responsible for the presence of EM3 grain sizes at NLK.

Post-depositional processes may also influence grain-size distribution. In large part this occurs due to chemical weathering which produces very fine silt and clay minerals (Xiao et al., 1995;Wang et al., 2006;Hao et al., 2008). Quartz grains are more resistant to weathering and remain largely unaltered during post-depositional processes. Consequently, quartz mineral grain size may be used as a more reliable proxy indicator of winter monsoon strength than other components (Sun et al., 2006;Sun et al., 2000b;Xiao et al., 1995). Figure. 6a shows the grain-size distribution curves of quartz grains isolated from primary loess (yellow) and paleosol (red) samples. The quartz modal grain size is finer in the paleosol than in the primary loess unit. From this we can deduce that wind strength was weaker during pedogenesis, and stronger during periods of primary loess deposition. The grain size distributions of bulk samples display similar characteristics with those of quartz samples mentioned above (Fig. 6b), since soil unit modal peaks (red and orange) are finer than those in the primary loess (blue and green). Therefore, we argue that wind strength, rather than the post-depositional pedogenesis, has the greatest influence on grain size distribution at NLK, and that EM3 was not produced by chemical weathering.

Fig. 6 Comparison of grain size distribution between purified quartz subsamples of paleosol and primary loess (a), and between bulk samples of paleosols and primary loess (b). Comparison of the grain size distribution between EM3 and samples from weak paleosol units (c).

The relative proportions of the end members down profile can yield information about temporal variability in wind dynamics. The fairly consistent proportions of EM3 within the loess units indicate it to represent continuous background dust through time (Vandenberghe, 2013). Proportions of EM1 and EM2 decrease noticeably within paleosol units relative to EM3 (Fig. 4). This indicates that variations in proportions of EM3 are mainly driven by variability in EM1 and EM2 (Vriend et al., 2011), but also that consistent background sedimentation of EM3 continued during weak pedogenesis (Fig. 6c). This characteristic is comparable with observations from the CLP (Zhang et al., 1999).

In addition, small peaks at c. 0.8 μm are also observed in the grain-size distribution curves of all three end members. The generation of these finest grain peaks may be due to post-depositional pedogenesis (Sun, 2006), especially for particles < 2 μm (Bronger and Heinkele, 1990;Sun, 2006). However, since the dominant modal peaks are much coarser, weaker post-depositional weathering as suggested by MS is unlikely to have had a significant influence on the populations of EM1, EM2 or EM3 at NLK. Other potential sources include transportation as aggregates or by the finest grains adhering to coarser particles during transport. Regardless of cause, these particles are unlikely to yield meaningful information about wind regime variability or links to climate systems since they do not yield a clear independent end member peak.

5.3 Aeolian dust dynamics in eastern Central Asia: links to atmospheric systems

Variations in grain size through time at NLK were largely driven by changes in wind strength, without substantial influence of post-depositional pedogenesis. At NLK, grain size is therefore an indicator of loess response to climatic systems.

The three end members are interpreted to represent different depositional processes which operated throughout the accumulation of the deposit. The finer EM3 is interpreted to represent constant background dust, which continued to accumulate throughout periods of relative stability and pedogenesis. The coarser populations, EM1 and EM2, were transported by low-level winds during major dust storms. EM1 is most likely the most sensitive recorder of wind intensity, since EM2 is less sensitive to wind speeds than EM1 by observation of variations in EM2 proportions throughout L1S1 and L1L2 (Fig. 4).

Fig. 7 Comparison between EM1 grain size variability and the timing of glacial advances in the Tien Shan (Koppes et al. 2008; Owen and Dortch, 2014); stable oxygen isotope variations from the Greenland ice cores (Rasmussen et al., 2014); mean grain size (MGS) record of the Jingyuan loess section from the CLP (Sun et al., 2010) and; U-ratio (15.6–63.4 μm/5.61–15.6 μm) of the SE Kazakhstan loess (Machalett et al., 2008). 5-point running average was performed for the intervals with higher sedimentary rate on EM1 curve (red line).

From published OSL data (Song et al., 2015), we used linear regression (Stevens et al., 2016) to construct age–depth relationships over intervals of visually similar sedimentation rate (Fig. S4 and Table S1). We assessed the degree of correlation between wind strength variability in the Ili Valley (NLK), as represented by the proportions of EM1, with the stable oxygen isotope record from the Greenland ice cores representing North Atlantic paleoclimate (Rasmussen et al., 2014), the mean grain size (MGS) record of the Jingyuan loess section from the CLP (Sun et al., 2010), U-ratio (15.6–63.4 μm/5.61–15.6 μm) of the Remizovka loess section in SE Kazakhstan (Machalett et al.,

2008), and glacial advances in the Tian Shan (Owen and Dortch, 2014;Koppes et al., 2008) (Fig. 7).

EM1 occurs in higher proportions during mid-MIS3, with a higher rate of sedimentary accumulation (Fig. 7). Glaciers in the region expanded during early- and late-MIS3 (Owen and Dortch, 2014). The apparent chronological link between increased primary loess accumulation and glacial expansion in the region contrasts with trends elsewhere indicating increased dust accumulation during dry-windy glacial conditions, and pedogenesis under comparatively wetter interglacial conditions (Stevens et al., 2013;Sun et al., 2010;Ding et al., 2002;Dodonov and Baiguzina, 1995). Our observations suggest a seesaw relationship between increased loess accumulation and glacial expansion during MIS3 (Fig. 7), a model supported by Youn et al. (2014). Moisture availability appears to be the dominant factor controlling glacier growth in Central Asia, especially for glaciers in the Tian Shan (Zech, 2012;Koppes et al., 2008). We infer, therefore, that moisture had an important impact on accumulation of dust in the study area during MIS3 in particular.

Central Asia is variably influenced by the Asian monsoon from the south (Dettman et al., 2001;Cheng et al., 2012), the mid-latitude westerlies (Vandenberghe et al., 2006), the Siberian high-pressure systems from the northeast (Youn et al., 2014), and the polar front from the north (Machalett et al., 2008). The Asian high mountains largely inhibit the intrusion of Asian (Indian and East Asian) monsoons to the region, since the Ili Valley is sheltered to the northeast, east and south. Studies of the oxygen isotopic composition of precipitation in the Tian Shan Mountains region support this geographic situation by indicating a stronger connection with westerly circulation than with the Asian summer monsoon (Liu et al., 2015;Chen et al., 2016).

Modern satellite data indicates that dust storm development in Ili river valley is closely linked with southward-moving high-latitude air masses (Ye et al., 2003). The large, cold Siberian High pressure system is at the north-northeast of our study area, centring between 40°N and 65°N, 80°E and 120°E (cf. Fig. 3 in Huang et al. (2011)). The Siberian anticyclone dominates winter and spring climate over Eurasia (Sahsamanoglou et al., 1991;Savelieva et al., 2000;Panagiotopoulos et al., 2005;Gong and Ho, 2002;Obreht et al., 2017). Although the influence of the Siberian High has been shown to decrease westward from the CLP (Vandenberghe et al., 2006), wind strength and frequency over the Aral Sea in western central Asia during the Holocene was nevertheless associated with the intensity of the Siberian High pressure system (Feng et al., 2011;Sorrel et al., 2007). Obreht et al. (2017) even hypothesized increased influence of the Siberian High during MIS 3 over the Lower Danube Basin in SE Europe, although this has yet to be substantiated. Moreover, the Siberian High was considered to be one of the most important influences on dust deposition based on the results of long-term monitoring over Central Asia between 2003 and 2010 (Groll et al., 2013).

Increases in modal grain-size from the CLP are also linked to a strengthened East Asian winter monsoon due to intensification of the Siberian High (Ding et al., 1995;Hao et al., 2012). Therefore, the grain-size record from the Chinese loess is a likely indicator of Siberian High intensity. We use the Jingyuan loess section as a point of comparison in our study, because it is a high resolution record located in the northwestern CLP, with high sedimentation rate, and thus the likelihood of preservation of millennial-scale oscillations. We compared secular trends between the EM1 proportions and MGS data from Jingyuan over the last glacial period (Sun et al., 2010). Similarities can be observed (Fig. 7); coarser grain sizes and higher sedimentation rates are observed during mid-MIS3 (Sun et al., 2010), with the opposite occurring in early- and late-MIS3. This supports a common Eurasian atmospheric forcing pattern - the Siberian High - driving the climate evolution of

463 the Ili Basin and CLP during that time period.

464 By comparison, the Last Glacial Maximum (LGM) witnesses significantly different trends,
465 despite increased sedimentation rates (Sun et al., 2010) (Fig. 7). EM1 proportions decrease
466 particularly during the early LGM. We attribute this to a reduction in sediment supply, possibly
467 linked to permafrost development in the Ili Basin and Kazakhstan steppe (Fig. 1) (Zhao et al.,
468 2014;Vandenberghe et al., 2014). Reduced sediment supply therefore limits the degree to which
469 grain-size characteristics can reliably indicate wind strength during the LGM.

470 Machalett et al. (2008), presenting data from the Remizovka site in the more open western Ili
471 Basin, argued that the Arctic polar front, expanding southward in winter and retracting northward
472 in summer, most likely increased the frequency and strength of cyclonic storms due to higher
473 temperature and humidity gradients created between colder polar air and warmer tropical air
474 (Harman, 1991). They hypothesized that this climate system was the predominant influence on dust
475 transport and loess accumulation during cold phases along the Kyrgyz (southern) Tian Shan
476 piedmont. While this may have been the case at Remizovka, it is unlikely to have affected NLK in
477 the eastern Ili Basin, however, since the eastern basin is much more sheltered due to the position of
478 the mountain ranges (Fig. 1a).

479 To assess spatial variability in climatic influence across the Ili Basin, we compare EM1 curve
480 with U-ratio (15.6–63.4 μm/5.61–15.6 μm) of the polar-front-influenced Remizovka loess. We
481 observe minimal similarities in the curves. These disparities suggest that two different atmospheric
482 forcing patterns controlled loess accumulation from one end of the Ili Basin to the other. The
483 differences appear to be particularly clear over MIS3 (Fig. 7), although problems with chronological
484 integrity at the Remizovka site need to be resolved (Fitzsimmons et al., 2016) before we can argue
485 this with confidence. In addition, U-ratios decrease during the LGM (Fig. 7), supporting our
486 hypothesis that the development of permafrost limits the availability of source sediments for loess
487 in this region.

488 We argue that the Siberian high-pressure system exerts a significant influence on wind
489 dynamics and loess deposition in the eastern Ili Basin. It is evident that the strongest winds at NLK
490 mainly blow from the west (Table S2), although northerly high-latitude air masses with potential
491 for short-term dust transport can enter the Ili Basin by deflection around the northern Tianshan
492 mountains (Fig. S5).

493 Enhanced evaporation, coupled with strengthened westerly winds, would bring more humid
494 and warmer conditions to ACA during the Holocene (Zhang et al., 2016). Karger et al. (2016)
495 reconstructed the dynamics of the westerlies in the Ili Basin, proposing a rain belt which seasonally
496 migrates towards the south and north in autumn and summer, respectively. A strengthened Siberian
497 High would push the mid-latitude Westerlies pathways further to the south, resulting in comparably
498 drier conditions in northeastern Central Asia (e.g. Tian Shan) but wetter conditions in southwestern
499 Central Asia (Pamir) (Lei et al., 2014;Wolff et al., 2017). The intensity and geographical position of
500 the Siberian High would most likely impact precipitation and atmospheric circulation patterns
501 (meridional or zonal) in the mid-latitudes of Central Asia (Panagiotopoulos et al., 2005). It is
502 therefore most likely that the mid-latitude Westerlies controlled broad-scale patterns of moisture
503 variation across ACA broadly (Huang et al., 2015;Li et al., 2011;Cai et al., 2017), whereas the
504 eastern Ili Basin experienced the combined influence of the Siberian High and mid-latitude
505 Westerlies system.

506 Comparison of EM1 proportions with variability in GISP $\delta^{18}O$ suggests that our grain-size

proxy data may correlate with abrupt events, such as North Atlantic Heinrich events H1 to H6 (Fig. 7), although this correlation cannot yet be better constrained due to limitations in the chronological dataset. Some of the peaks in EM1 curve correspond to troughs in GISP $\delta^{18}O$ curve (black arrows in Fig. 7) outside Heinrich events, yet many do not (pink dashed lines in Fig. 7). Potential causes of this discrepancy may lie in variability in local source availability and wind dynamics at certain points in time.

Comparisons between the eastern Ili Basin and Chinese Loess Plateau loess further elucidates complexity in the climatic signal preserved in the ACA. The NLK EM1 proportions in the Ili Basin yield lower variability than the Jingyuan MGS on the CLP, particularly during H2 and H5 (Fig. 7). We attribute these differences to local source sediment availability at NLK. EM1 supply to NLK was reduced during H2 due to the development of permafrost, and during H5 due to increased vegetation cover associated with more humid conditions inhibiting coarse-grain entrainment (Fig. 7). By contrast, the relatively more arid mid-MIS 3, indicated by glacial retreat in the Tian Shan, may have decreased vegetation cover and increased entrainment potential and transport to NLK (Fig. 7); these conditions and this trend was also observed in the NE-TP (Vriend et al., 2011). The differences may be because the loess records in our study area represent a response not only to hemispheric climate systems, but also to local influences such as local atmospheric circulation and topography. Since the sedimentary response to changing climate conditions in more arid Central Asia is different to that of the more temperate European loess (Rousseau et al., 2007), we must be careful about investigating the mechanisms of aeolian dynamics and loess accumulation in our paleoclimatic interpretations of ACA loess archives.

Many studies have speculate that millennial-scale oscillations represent a teleconnection between the North Atlantic and East Asia (e.g. Porter and An, 1995; Yang and Ding, 2014), although the dynamics involved are poorly understood. Porter and An (1995) and Sun et al. (2012) suggested, based on CLP loess physical characteristics, that a strong influence from the westerlies resulted in transport of the North Atlantic signal to East Asia. Conversely, Yang and Ding (2014) proposed that millennial-scale North Atlantic climate signals might have been transmitted to the Siberian High via the Barents and Kara Sea ice sheets, and were propagated eastwards to the CLP via the winter monsoon system. In the western CLP (Chen et al., 1997a), for example, evidence of millennial-scale (likely Heinrich) events are preserved within the loess stratigraphy during phases of strong winter monsoon in China; however, not all of the strong winter monsoon events in China correlate with Heinrich events in the North Atlantic, so challenging the Yang and Ding (2014) hypothesis.

Stronger datasets from Central Asia may provide the missing link for understanding climate teleconnections between the two extreme ends of the Eurasian continent. In doing so, however, the scale of the "Central Asian" region must be taken into account. At Darai Kalon in Tajikistan, 1200 km southwest of NLK, the mid-latitude westerlies clearly have a strong influence on dust transport and loess accumulation; Atlantic signals are clearly identified in grain size variations, especially during full glacial phases (Vandenberghe et al., 2006). Since the CLP lies at a similar latitude to Darai Kalon, mid-latitude Westerlies have the potential to transport North Atlantic climate signals to East Asia. By contrast, since NLK is located substantially further north than Darai Kalon and the CLP, the Siberian High exerts a greater influence on wind dynamics and therefore loess deposits. A strengthened Siberian High would effect a southward shift of the mid-latitude Westerlies pathways; under such conditions, NLK would be less strongly influenced by the mid-latitude westerlies. This argument is further supposed by the lack of correlation between NLK EM1 proportions and GISP

$\delta^{18}O$ values during relatively mild interstadial periods (Dansgaard-Oeschger cycles) when the mid-latitude westerlies shift northwards (Fig. 7). Therefore, NLK provides a strategic location for investigating the potential role of the Siberian High in transmitting North Atlantic climate signals to East Asia. The preservation of North Atlantic several millennial-scale Heinrich events at NLK supports the argument for the influence of the Siberian High as argued by Yang and Ding (2014).

Conclusion

Our data from NLK in the eastern Ili Basin provide a paleoenvironmental record over the last c. 70 ky. The magnetic properties of the loess do not correlate with pedogenesis in this section; rather, wind strength is mainly responsible for variations in physical characteristics over the last glacial period.

Three grain-size end members were identified at NLK: EM1 (mode size at 47.5 μm), EM2 (33.6 μm) and EM3 (18.9 μm). They each indicate different kinds of depositional processes which operated throughout the accumulation of the loess. EM1 and EM2 represent grain-size fractions transported from proximal sources in short-term, near-surface suspension during dust outbreaks, and may have the same origin. While wind strength controls their relative proportions, EM1 is the most sensitive recorder of wind strength. EM3 represents continuous background dust under non-dust storm conditions.

The Siberian High-pressure system predominates in the eastern Ili Basin during cold phases, which leads to dust transport and increased loess accumulation at NLK. Many rapid cooling events, including 6 Heinrich events, were imprinted in the NLK loess. Our grain size data support the argument that the Siberian High plays a significant role in transporting North Atlantic climatic signals to East Asia via ice sheets in the high northern latitudes.

Acknowledgements

The project is supported by the National Basic Research Program of China (Nos: 2016YFA0601902, 2013CB955904), Natural Science Foundation of China (Nos: 41572162, 41290253), and International Partnership Program of Chinese Academy of Science [No: 132B61KYS20160002]. The authors thank Yun Li and Junchao Dong from Institute of Earth Environment, Chinese Academy of Sciences, for their assistances in sampling and experiment, and Jia Li from Xiamen University for her assistance in mathematical treatment.

References

Antoine, P., Rousseau, D.-D., Moine, O., Kunesch, S., Hatté, C., Lang, A., Tissoux, H., and Zöller, L.: Rapid and cyclic aeolian deposition during the Last Glacial in European loess: a high-resolution record from Nussloch, Germany, Quaternary Sci Rev, 28, 2955-2973, 2009.

Beget, J. E., and Hawkins, D. B.: Influence of Orbital Parameters on Pleistocene Loess Deposition in Central Alaska, Nature, 337, 151-153, DOI 10.1038/337151a0, 1989.

Bokhorst, M. P., Vandenberghe, J., Sumegi, P., Lanczont, M., Gerasimenko, N. P., Matviishina, Z. N., Markovic, S. B., and Frechen, M.: Atmospheric circulation patterns in central and eastern Europe during the Weichselian Pleniglacial inferred from loess grain-size records, Quatern Int, 234, 62-74, 10.1016/j.quaint2010.07.018, 2011.

Bond, G., Heinrich, H., Broecker, W., Labeyrie, L., Mcmanus, J., Andrews, J., Huon, S., Jantschik, R., Clasen, S., Simet, C., Tedesco, K., Klas, M., Bonani, G., and Ivy, S.: Evidence for massive discharges of icebergs into the North Atlantic Ocean during the last glacial period, Nature, 360, 245–249, 1992.

Bronger, A., and Heinkele, T.: Mineralogical and clay mineralogical aspects of loess research,

595 Quatern Int, 7, 37-51, 1990.
596 Buggle, B., Hambach, U., Glaser, B., Gerasimenko, N., Markovic, S., Glaser, I., and Zöller, L.:
597 Stratigraphy, and spatial and temporal paleocliamtic trends in Southeastern/Eastern European loess-
598 paleosol sequences, Quatern Int, 196, 86–106, 2009.
599 Buggle, B., Hambach, U., Muller, K., Zoller, L., Markovic, S. B., and Glaser, B.: Iron mineralogical
600 proxies and Quaternary climate change in SE-European loess-paleosol sequences, Catena, 117, 4-
601 22, 10.1016/j.catena.2013.06.012, 2014.
602 Cai, Y. J., Chiang, J. C. H., Breitenbach, S. F. M., Tan, L. C., Cheng, H., Edwards, R. L., and An, Z.
603 S.: Holocene moisture changes in western China, Central Asia, inferred from stalagmites,
604 Quaternary Sci Rev, 158, 15-28, 2017.
605 Chen, F., Bloemendal, J., Wang, J., Li, J., and Oldfield, F.: High-resolution multi-proxy climate
606 records from Chinese loess: evidence for rapid climatic changes over the last 75 kyr,
607 Palaeogeography, Palaeoclimatology, Palaeoecology, 130, 323-335, 1997a.
608 Chen, F. H., Bloemendal, J., Wang, J. M., Li, J. J., and Oldfield, F.: High-resolution multi-proxy
609 climate records from Chinese loess, evidence for rapid climatic changes over the last 75 kyr,
610 Palaeogeogr Palaeocl, 130, 323-335, 1997b.
611 Chen, F. H., Jia, J., Chen, J. H., Li, G. Q., Zhang, X. J., Xie, H. C., Xia, D. S., Huang, W., and An,
612 C. B.: A persistent Holocene wetting trend in arid central Asia, with wettest conditions in the late
613 Holocene, revealed by multi-proxy analyses of loess-paleosol sequences in Xinjiang, China,
614 Quaternary Sci Rev, 146, 134-146, 2016.
615 Cheng, H., Zhang, P. Z., Spotl, C., Edwards, R. L., Cai, Y. J., Zhang, D. Z., Sang, W. C., Tan, M.,
616 and An, Z. S.: The climatic cyclicity in semiarid-arid central Asia over the past 500,000 years,
617 Geophys Res Lett, 39, Artn L01705
618 10.1029/2011gl050202, 2012.
619 Dansgaard, W., Johnsen, S. J., Clausen, H. B., Hvidberg, C. S., and Steffensen, J. P.: Evidence for
620 general instability of past climate from a 250-kyr ice-core record, Nature, 364, 218– 220, 1993.
621 Derbyshire, E., Meng, X. M., and Kemp, R. A.: Provenance, transport and characteristics of modern
622 aeolian dust in western Gansu Province, China, and interpretation of the Quaternary loess record,
623 Journal of Arid Environments, 39, 497-516, DOI 10.1006/jare.1997.0369, 1998.
624 Dettman, D. L., Kohn, M. J., Quade, J., Ryerson, F. J., Ojha, T. P., and Hamidullah, S.: Seasonal
625 stable isotope evidence for a strong Asian monsoon throughout the past 10.7 m.y., Geology, 29, 31-
626 34, Doi 10.1130/0091-7613(2001)029<0031:Ssiefa>2.0.Co;2, 2001.
627 Ding, Z., Liu, T., Rutter, N. W., Yu, Z., Guo, Z., and Zhu, R.: Ice-volume forcing of East Asian
628 winter monsoon variations in the past 800,000 years, Quaternary Res, 44, 149-159, 1995.
629 Ding, Z. L., Sun, J. M., Rutter, N. W., Rokosh, D., and Liu, T. S.: Changes in sand content of loess
630 deposits along a north-south transect of the Chinese Loess Plateau and the implications for desert
631 variations, Quaternary Research, 52, 56-62, DOI 10.1006/qres.1999.2045, 1999.
632 Ding, Z. L., Ranov, V., Yang, S. L., Finaev, A., Han, J. M., and Wang, G. A.: The loess record in
633 southern Tajikistan and correlation with Chinese loess, Earth Planet Sc Lett, 200, 387-400, doi: DOI:
634 10.1016/S0012-821X(02)00637-4, 2002.
635 Ding, Z. L., Derbyshire, E., Yang, S. L., Sun, J. M., and Liu, T. S.: Stepwise expansion of desert
636 environment across northern China in the past 3.5 Ma and implications for monsoon evolution,
637 Earth Planet Sc Lett, 237, 45-55, 10.1016/j.epsl.2005.06.036, 2005.
638 DiPietro, L. M., Driese, S. G., Nelson, T. W., and Harvill, J. L.: Variations in late Quaternary wind

intensity from grain-size partitioning of loess deposits in the Nenana River Valley, Alaska, Quaternary Research, 87, 258-274, 2017.
Dodonov, A. E., and Baiguzina, L. L.: Loess stratigraphy of Central Asia: Palaeoclimatic and palaeoenvironmental aspects, Quaternary Sci Rev, 14, 707-720, http://dx.doi.org/10.1016/0277-3791(95)00054-2, 1995.
Dodonov, A. E., Sadchikova, T. A., Sedov, S. N., Simakova, A. N., and Zhou, L. P.: Multidisciplinary approach for paleoenvironmental reconstruction in loess-paleosol studies of the Darai Kalon section, Southern Tajikistan, Quatern Int, 152, 48-58, 10.1016/j.quaint.2005.12.001, 2006.
Feng, Z. D., Ran, M., Yang, Q. L., Zhai, X. W., Wang, W., Zhang, X. S., and Huang, C. Q.: Stratigraphies and chronologies of late Quaternary loess-paleosol sequences in the core area of the central Asian arid zone, Quatern Int, 240, 156-166, doi: 10.1016/j.quaint.2010.10.019, 2011.
Fitzsimmons, K. E., Sprafke, T., Zielhofer, C., Günter, C., Deom, J. M., Sala, R., and Iovita, R.: Loess accumulation in the Tian Shan piedmont: Implications for palaeoenvironmental change in arid Central Asia, Quatern Int, http://dx.doi.org/10.1016/j.quaint.2016.1007.1041, 2016.
Folk, R. L., and Ward, W. C.: Brazos River bar: a study in the significance of grain size parameters, Journal of Sedimentary Research, 27, 3-26, 1957.
Gong, D. Y., and Ho, C. H.: The Siberian High and climate change over middle to high latitude Asia, Theor Appl Climatol, 72, 1-9, 2002.
Grimley, D. A., and Arruda, N. K.: Observations of magnetite dissolution in poorly drained soils, Soil Sci, 172, 968-982, 10.1097/ss.0b013e3181586b77, 2007.
Groll, M., Opp, C., and Aslanov, I.: Spatial and temporal distribution of the dust deposition in Central Asia - results from a long term monitoring program, Aeolian Res, 9, 49-62, 2013.
Hao, Q., Wang, L., Oldfield, F., Peng, S., Qin, L., Song, Y., Xu, B., Qiao, Y., Bloemendal, J., and Guo, Z.: Delayed build-up of Arctic ice sheets during 400,000-year minima in insolation variability, Nature, 490, 393-396, 2012.
Hao, Q. Z., Oldfield, F., Bloemendal, J., and Guo, Z. T.: Particle size separation and evidence for pedogenesis in samples from the Chinese Loess Plateau spanning the past 22 m.y., Geology, 36, 727-730, 10.1130/G24940a.1, 2008.
Harman, J. R.: Synoptic Climatology of the Westerlies: Process and Patterns, Association of American Geographers, Washington, DC, 1991.
Heller, F., and Liu, T. S.: Magnetism of Chinese Loess Deposits, Geophys J Roy Astr S, 77, 125-&, DOI 10.1111/j.1365-246X.1984.tb01928.x, 1984.
Heller, F., Shen, C. D., Beer, J., Liu, X. M., Liu, T. S., Bronger, A., Suter, M., and Bonani, G.: Quantitative Estimates of Pedogenic Ferromagnetic Mineral Formation in Chinese Loess and Paleoclimatic Implications, Earth Planet Sc Lett, 114, 385-390, Doi 10.1016/0012-821x(93)90038-B, 1993.
Heller, F., and Evans, M. E.: Loess magnetism, Reviews of Geophysics, 33, 211–240, 1995.
Huang, W., Chen, J. H., Zhang, X. J., Feng, S., and Chen, F. H.: Definition of the core zone of the "westerlies-dominated climatic regime", and its controlling factors during the instrumental period, Sci China Earth Sci, 58, 676-684, 10.1007/s11430-015-5057-y, 2015.
Huang, X. T., Oberhansli, H., von Suchodoletz, H., and Sorrel, P.: Dust deposition in the Aral Sea: implications for changes in atmospheric circulation in central Asia during the past 2000 years, Quaternary Sci Rev, 30, 3661-3674, 2011.

Jacobs, P. M., Mason, J. A., and Hanson, P. R.: Mississippi Valley regional source of loess on the southern Green Bay Lobe land surface, Wisconsin, Quaternary Research, 75, 574-583, 10.1016/j.yqres.2011.02.003, 2011.
Jia, J., Xia, D. S., Wei, H. T., Wang, B., and Liu, X. B.: A magnetic investigation of a loess/paleosol sequences record in Ili area, Front Earth Sci-Prc, 4, 259-268, 10.1007/s11707-010-0115-4, 2010.
Jia, J., Xia, D. S., Wang, B., Wei, H. T., and Liu, X. B.: Magnetic investigation of Late Quaternary loess deposition, Ili area, China, Quatern Int, 250, 84-92, 10.1016/j.quaint.2011.06.018, 2012.
Karger, D. N., Conrad, O., Böhner, J., Kawohl, T., Kreft, H., Soria-Auza, R. W., Zimmermann, N., Linder, H. P., and Kessler, M.: Climatologies at high resolution for the Earth land surface areas, arXiv:1607.00217, 2016.
Konert, M., and Vandenberghe, J.: Comparison of laser grain size analysis with pipette and sieve analysis: A solution for the underestimation of the clay fraction, Sedimentology, 44, 523-535, DOI 10.1046/j.1365-3091.1997.d01-38.x, 1997.
Koppes, M., Gillespie, A. R., Burke, R. M., Thompson, S. C., and Stone, J.: Late Quaternary glaciation in the Kyrgyz Tien Shan, Quaternary Sci Rev, 27, 846-866, 10.1016/j.quascirev.2008.01.009, 2008.
Lei, Y. B., Tian, L. D., Bird, B. W., Hou, J. Z., Ding, L., Oimahmadov, I., and Gadoev, M.: A 2540-year record of moisture variations derived from lacustrine sediment (Sasikul Lake) on the Pamir Plateau, Holocene, 24, 761-770, 2014.
Li, G. Q., Rao, Z. G., Duan, Y. W., Xia, D. S., Wang, L. B., Madsen, D. B., Jia, J., Wei, H. T., Qiang, M. R., Chen, J. H., and Chen, F. H.: Paleoenvironmental changes recorded in a luminescence dated loess/paleosol sequence from the Tianshan Mountains, arid central Asia, since the Penultimate Glaciation, Earth Planet Sc Lett, 448, 1-12, 10.1016/j.epsl.2016.05.008, 2016a.
Li, J.: Climate in Xinjiang, in, China Meteorological Press, Beijing, 1-205 (in Chinese), 1991.
Li, X., Zhao, K., Dodson, J., and Zhou, X.: Moisture dynamics in central Asia for the last 15 kyr: new evidence from Yili Valley, Xinjiang, NW China, Quaternary Sci Rev, 30, 3457-3466, 2011.
Li, Y., Song, Y., Lai, Z., Han, L., and An, Z.: Rapid and cyclic dust accumulation during MIS 2 in Central Asia inferred from loess OSL dating and grain-size analysis, Scientific Reports, 6, DOI: 10.1038/srep32365, 2016b.
Li, Y., Song, Y. G., Chen, X. L., Li, J. C., Mamadjanov, Y., and Aminov, J.: Geochemical composition of Tajikistan loess and its provenance implications, Palaeogeogr Palaeocl, 446, 186-194, 10.1016/j.palaeo.2016.01.025, 2016c.
Lin, Y. C., Mu, G. J., Xu, L. S., and Zhao, X.: The origin of bimodal grain-size distribution for aeolian deposits, Aeolian Research, 20, 80-88, 10.1016/j.aeolia.2015.12.001, 2016.
Liu, Q. S., Deng, C. L., Torrent, J., and Zhu, R. X.: Review of recent developments in mineral magnetism of the Chinese loess, Quaternary Sci Rev, 26, 368-385, 10.1016/j.quascirev.2006.08.004, 2007.
Liu, Q. S., Roberts, A. P., Larrasoana, J. C., Banerjee, S. K., Guyodo, Y., Tauxe, L., and Oldfield, F.: Environmental Magnetism: Principles and Applications, Reviews of Geophysics, 50, Artn Rg4002
10.1029/2012rg000393, 2012.
Liu, T. S.: Loess and the environment, Ocean Press, Beijing, 1985b.
Liu, X., Liu, Z., Lü, B., Marković, S., Chen, J., Guo, H., Ma, M., Zhao, G., and Feng, H.: The magnetic properties of Serbian loess and its environmental significance, Chinese Science Bulletin,

1-11, 2013.
Liu, X. K., Rao, Z. G., Zhang, X. J., Huang, W., Chen, J. H., and Chen, F. H.: Variations in the oxygen isotopic composition of precipitation in the Tianshan Mountains region and their significance for the Westerly circulation, J Geogr Sci, 25, 801-816, 2015.
Liu, X. M., Shaw, J., Liu, T. S., Heller, F., and Yuan, B. Y.: Magnetic Mineralogy of Chinese Loess and Its Significance, Geophys J Int, 108, 301-308, DOI 10.1111/j.1365-246X.1992.tb00859.x, 1992.
Liu, X. M., Rolph, T., Bloemendal, J., Shaw, J., and Liu, T. S.: Remanence characteristics of different magnetic grain size categories at Xifeng, central Chinese Loess Plateau, Quaternary Research, 42, 162-165, 1994.
Liu, X. M., Hesse, P., Rolph, T., and Begét, J. E.: Properties of magnetic mineralogy of Alaskan loess: evidence for pedogenesis, Quatern Int, 62, 93-102, 1999.
Lu, H. Y., and An, Z. S.: Pretreatment methods in loess–palaeosol granulometry, Chinese Science Bulletin, 42, 237-240, 1997.
Lu, H. Y., and An, Z. S.: Paleoclimatic significance of grain size of loess-palaeosol deposit in Chinese Loess Plateau, Sci China Ser D, 41, 626-631, Doi 10.1007/Bf02878745, 1998.
Machalett, B., Frechen, M., Hambach, U., Oches, E. A., Zoller, L., and Markovic, S. B.: The loess sequence from Remisowka (northern boundary of the Tien Shan Mountains, Kazakhstan) - Part I: Luminescence dating, Quatern Int, 152, 192-201, 10.1016/j.quaint.2005.12.014, 2006.
Machalett, B., Oches, E. A., Frechen, M., Zoller, L., Hambach, U., Mavlyanova, N. G., Markovic, S. B., and Endlicher, W.: Aeolian dust dynamics in central Asia during the Pleistocene: Driven by the long-term migration, seasonality, and permanency of the Asiatic polar front, Geochem Geophy Geosy, 9, Artn Q08q09
10.1029/2007gc001938, 2008.
Maher, B., and Thompson, R.: Paleoclimatic significance of the mineral magnetic record of the Chinese loess and paleosols, Quaternary Research, 37, 155–170, 1992.
Maher, B. A., and Taylor, R. M.: Formation of Ultrafine-Grained Magnetite in Soils, Nature, 336, 368-370, DOI 10.1038/336368a0, 1988.
Maher, B. A., and Thompson, R.: Paleorainfall reconstructions from pedogenic magnetic susceptibility variations in the Chinese loess and paleosols, Quaternary Research, 44, 383-391, DOI 10.1006/qres.1995.1083, 1995.
Maher, B. A.: Magnetic properties of modern soils and Quaternary loessic paleosols: paleoclimatic implications, Palaeogeogr Palaeocl, 137, 25-54, Doi 10.1016/S0031-0182(97)00103-X, 1998.
Maher, B. A.: Palaeoclimatic records of the loess/palaeosol sequences of the Chinese
Loess Plateau, Quaternary Sci Rev, 154, 23-84, 2016.
Mason, J. A., Jacobs, P. M., Greene, R. S. B., and Nettleton, W. D.: Sedimentary aggregates in the Peoria Loess of Nebraska, USA, Catena, 53, 377-397, 10.1016/S0341-8162(03)00073-0, 2003.
Muhs, D. R., and Bettis, E. A.: Quaternary loess-paleosol sequences as examples of climate-driven sedimentary extremes, Special Papers-Geological Society of America, 53-74, 2003.
Muhs, D. R.: The geologic records of dust in the Quaternary, Aeolian Research, 9, 3-48, 2013.
Nawrocki, J., Wojcik, A., and Bogucki, A.: The magnetic susceptibility record in the Polish and western Ukrainian loess-palaeosol sequences conditioned by palaeoclimate, Boreas, 25, 161-169, 1996.
Nottebaum, V., Lehmkuhl, F., Stauch, G., Hartmann, K., Wunnemann, B., Schimpf, S., and Lu, H. Y.: Regional grain size variations in aeolian sediments along the transition between Tibetan

771 highlands and north-western Chinese deserts - the influence of geomorphological settings on aeolian
772 transport pathways, Earth Surf Proc Land, 39, 1960-1978, 10.1002/esp.3590, 2014.
773 Nottebaum, V., Stauch, G., Hartmann, K., Zhang, J. R., and Lehmkuhl, F.: Unmixed loess grain size
774 populations along the northern Qilian Shan (China): Relationships between geomorphologic,
775 sedimentologic and climatic controls, Quatern Int, 372, 151-166, 10.1016/j.quaint.2014.12.071,
776 2015.
777 Obreht, I., Zeeden, C., Schulte, P., Hambach, U., Eckmeier, E., Timar-Gabor, A., and Lehmkuhl, F.:
778 Aeolian dynamics at the Orlovat loess-paleosol sequence, northern Serbia, based on detailed textural
779 and geochemical evidence, Aeolian Research, 18, 69-81, 2015.
780 Obreht, I., Hambach, U., Veres, D., Zeeden, C., Bösken, J., Stevens, T., Marković, S. B., Klasen, N.,
781 Brill, D., and Burow, C.: Shift of large-scale atmospheric systems over Europe during late MIS 3
782 and implications for Modern Human dispersal, Scientific Reports, 7, 2017.
783 Owen, L. A., and Dortch, J. M.: Nature and timing of Quaternary glaciation in the Himalayan-
784 Tibetan orogen, Quaternary Sci Rev, 88, 14-54, 10.1016/j.quascirev.2013.11.016, 2014.
785 Panagiotopoulos, F., Shahgedanova, M., Hannachi, A., and Stephenson, D. B.: Observed trends and
786 teleconnections of the Siberian high: A recently declining center of action, J Climate, 18, 1411-1422,
787 2005.
788 Porter, S. C., and An, Z. S.: Correlation between climate events in the North-Atlantic and China
789 during Last Glaciation, Nature, 375, 305-308, Doi 10.1038/375305a0, 1995.
790 Prins, M. A., and Vriend, M.: Glacial and interglacial eolian dust dispersal patterns across the
791 Chinese Loess Plateau inferred from decomposed loess grain-size records, Geochem Geophy Geosy,
792 8, Artn Q07q05
793 10.1029/2006gc001563, 2007.
794 Prins, M. A., Vriend, M., Nugteren, G., Vandenberghe, J., Lu, H. Y., Zheng, H. B., and Weltje, G. J.:
795 Late Quaternary aeolian dust input variability on the Chinese Loess Plateau: inferences from
796 unmixing of loess grain-size records, Quaternary Sci Rev, 26, 230-242,
797 10.1016/j.quascirev.2006.07.002, 2007.
798 Prins, M. A., Zheng, H. B., Beets, K., Troelstra, S., Bacon, P., Kamerling, I., Wester, W., Konert,
799 M., Huang, X. T., Ke, W., and Vandenberghe, J.: Dust supply from river floodplains: the case of the
800 lower Huang He (Yellow River) recorded in a loess-palaeosol sequence from the Mangshan Plateau,
801 J Quaternary Sci, 24, 75-84, 10.1002/jqs.1167, 2009.
802 Pye, K.: Aeolian Dust and Dust Deposits, in, Academic Press, London, 29-62, 1987.
803 Pye, K., and Zhou, L. P.: Late Pleistocene and Holocene Aeolian Dust Deposition in North China
804 and the Northwest Pacific-Ocean, Palaeogeogr Palaeocl, 73, 11-23, Doi 10.1016/0031-
805 0182(89)90041-2, 1989.
806 Pye, K.: The nature, origin and accumulation of loess, Quaternary Sci Rev, 14, 653-667, Doi
807 10.1016/0277-3791(95)00047-X, 1995.
808 Qiang, M., Lang, L., and Wang, Z.: Do fine-grained components of loess indicate westerlies:
809 Insights from observations of dust storm deposits at Lenghu (Qaidam Basin, China), Journal of Arid
810 Environments, 74, 1232-1239, 10.1016/j.jaridenv.2010.06.002, 2010.
811 Qin, X. G., Cai, B. G., and Liu, T. S.: Loess record of the aerodynamic environment in the east Asia
812 monsoon area since 60,000 years before present, J Geophys Res-Sol Ea, 110, Artn B01204
813 10.1029/2004jb003131, 2005.
814 Rasmussen, S. O., Bigler, M., Blockley, S. P., Blunier, T., Buchardt, S. L., Clausen, H. B., Cvijanovic,

I., Dahl-Jensen, D., Johnsen, S. J., Fischer, H., Gkinis, V., Guillevic, M., Hoek, W. Z., Lowe, J. J., Pedro, J. B., Popp, T., Seierstad, I. K., Steffensen, J. P., Svensson, A. M., Vallelonga, P., Vinther, B. M., Walker, M. J. C., Wheatley, J. J., and Winstrup, M.: A stratigraphic framework for abrupt climatic changes during the Last Glacial period based on three synchronized Greenland ice-core records: refining and extending the INTIMATE event stratigraphy, Quaternary Sci Rev, 106, 14-28, 10.1016/j.quascirev.2014.09.007, 2014.

Rea, D. K., Leinen, M., and Janecek, T. R.: Geologic Approach to the Long-Term History of Atmospheric Circulation, Science, 227, 721-725, DOI 10.1126/science.227.4688.721, 1985.

Rea, D. K., and Hovan, S. A.: Grain-Size Distribution and Depositional Processes of the Mineral Component of Abyssal Sediments - Lessons from the North Pacific, Paleoceanography, 10, 251-258, Doi 10.1029/94pa03355, 1995.

Rousseau, D. D., Sima, A., Antoine, P., Hatté, C., Lang, A., and Zöller, L.: Link between European and North Atlantic abrupt climate changes over the last glaciation, Geophys Res Lett, 34, 22, 2007.

Sahsamanoglou, H. S., Makrogiannis, T. J., and Kallimopoulos, P. P.: Some Aspects of the Basic Characteristics of the Siberian Anticyclone, Int J Climatol, 11, 827-839, 1991.

Savelieva, N. I., Semiletov, I. P., Vasilevskaya, L. N., and Pugach, S. P.: A climate shift in seasonal values of meteorological and hydrological parameters for Northeastern Asia, Prog Oceanogr, 47, 279-297, 2000.

Schettler, G., Shabunin, A., Kemnitz, H., Knoeller, K., Imashev, S., Rybin, A., and Wetzel, H. U.: Seasonal and diurnal variations in dust characteristics on the northern slopes of the Tien Shan - Grain-size, mineralogy, chemical signatures and isotope composition of attached nitrate, Journal of Asian Earth Sciences, 88, 257-276, 2014.

Smalley, I. J., Mavlyanova, N. G., Rakhmatullaev, K. L., Shermatov, M. S., Machalett, B., Dhand, K. O., and Jefferson, I. F.: The formation of loess deposits in the Tashkent region and parts of Central Asia; and problems with irrigation, hydrocollapse and soil erosion, Quatern Int, 152, 59-69, 10.1016/j.quaint.2005.12.002, 2006.

Song, Y., Zeng, M., Chen, X., Li, Y., Chang, H., An, Z., and Guo, X.: Abrupt climatic events recorded by the Ili loess during the last glaciation in Central Asia: Evidence from grain-size and minerals, Journal of Asian Earth Sciences, in press, https://doi.org/10.1016/j.jseaes.2017.1010.1040, 2017a.

Song, Y. G., Shi, Z. T., Fang, X. M., Nie, J. S., Naoto, I., Qiang, X. K., and Wang, X. L.: Loess magnetic properties in the Ili Basin and their correlation with the Chinese Loess Plateau, Sci China Earth Sci, 53, 419-431, 10.1007/s11430-010-0011-5, 2010.

Song, Y. G., Li, C. X., Zhao, J. D., Cheng, P., and Zeng, M. X.: A combined luminescence and radiocarbon dating study of the Ili loess, Central Asia, Quat Geochronol, 10, 2-7, 10.1016/j.quageo.2012.04.005, 2012.

Song, Y. G., Chen, X. L., Qian, L. B., Li, C. X., Li, Y., Li, X. X., Chang, H., and An, Z. S.: Distribution and composition of loess sediments in the Ili Basin, Central Asia, Quatern Int, 334, 61-73, 10.1016/j.quaint.2013.12.053, 2014.

Song, Y. G., Lai, Z. P., Li, Y., Chen, T., and Wang, Y. X.: Comparison between luminescence and radiocarbon dating of late Quaternary loess from the Ili Basin in Central Asia, Quat Geochronol, 30, 405-410, 10.1016/j.quageo.2015.01.012, 2015.

Song, Y. G., Li, Y., Li, Y., An, Z., Cheng, L., Sun, H., and Rustam, O.: North Atlantic Abrupt Climate Signals during the Last Glacial Period in Central Asia: Evidences from Aeolian Loess Sediments,

Acta Geologica Sinica - English Edition, 91, 1135-1136, 2017b.
Sorrel, P., Oberhansli, H., Boroffka, N., Nourgaliev, D., Dulski, P., and Rohl, U.: Control of wind strength and frequency in the Aral Sea basin during the late Holocene, Quaternary Res, 67, 371-382, 2007.
Stevens, T., Adamiec, G., Bird, A. F., and Lu, H. Y.: An abrupt shift in dust source on the Chinese Loess Plateau revealed through high sampling resolution OSL dating, Quaternary Sci Rev, 82, 121-132, 10.1016/j.quascirev.2013.10.014, 2013.
Stevens, T., Buylaert, J. P., Lu, H., Thiel, C., Murray, A., Frechen, M., Yi, S., and Zeng, L.: Mass accumulation rate and monsoon records from Xifeng, Chinese Loess Plateau, based on a luminescence age model, J Quaternary Sci, 31, 391-405, 2016.
Sun, D. H., Bloemendal, J., Rea, D. K., Vandenberghe, J., Jiang, F. C., An, Z. S., and Su, R. X.: Grain-size distribution function of polymodal sediments in hydraulic and aeolian environments, and numerical partitioning of the sedimentary components, Sediment Geol, 152, 263-277, Pii S0037-0738(02)00082-9
Doi 10.1016/S0037-0738(02)00082-9, 2002.
Sun, D. H., Chen, F. H., Bloemendal, J., and Su, R. X.: Seasonal variability of modern dust over the Loess Plateau of China, J Geophys Res-Atmos, 108, Artn 4665
10.1029/2003jd003382, 2003.
Sun, D. H., Bloemendal, J., Rea, D. K., An, Z. S., Vandenberghe, J., Lu, H. Y., Su, R. X., and Liu, T. S.: Bimodal grain-size distribution of Chinese loess, and its palaeoclimatic implications, Catena, 55, 325-340, 10.1016/S0341-8162(03)00109-7, 2004.
Sun, D. H.: Supper-fine grain size components in Chinese loess and their palaeoclimatic implication, Quaternary Sciences, 26, 928-936 (in Chinese with English abstract), 2006.
Sun, Y., Lu, H., and An, Z.: Grain size distribution of quartz isolated from Chinese loess1 paleosol, Chinese Science Bulletin, 45, 2296-2298, 2000a.
Sun, Y., Lu, H. Y., and An, Z. S.: Grain size of loess, palaeosol and Red Clay deposits on the Chinese Loess Plateau: Significance for understanding pedogenic alteration and palaeomonsoon evolution, Palaeogeogr Palaeocl, 241, 129-138, 10.1016/j.palaeo.2006.06.018, 2006.
Sun, Y., Clemens, S. C., Morrill, C., Lin, X., Wang, X., and An, Z.: Influence of Atlantic meridional overturning circulation on the East Asian winter monsoon, Nature Geoscience, 5, 46-49, 2012.
Sun, Y. B., Lu, H. Y., and An, Z. S.: Grain size distribution of quartz isolated from Chinese loess/paleosol, Chinese Science Bulletin, 45, 2296-2298, Doi 10.1007/Bf02886372, 2000b.
Sun, Y. B., Wang, X. L., Liu, Q. S., and Clemens, S. C.: Impacts of post-depositional processes on rapid monsoon signals recorded by the last glacial loess deposits of northern China, Earth Planet Sc Lett, 289, 171-179, 10.1016/j.epsl.2009.10.038, 2010.
Terhorst, B., Ottner, F., and Wriessnig, K.: Weathering intensity and pedostratigraphy of the Middle to Upper Pleistocene loess/palaeosol sequence of Wels-Aschet (Upper Austria), Quatern Int, 265, 142-154, 2012.
Tsoar, H., and Pye, K.: Dust Transport and the Question of Desert Loess Formation, Sedimentology, 34, 139-153, DOI 10.1111/j.1365-3091.1987.tb00566.x, 1987.
Ujvari, G., Kok, J. F., Varga, G., and Kovacs, J.: The physics of wind-blown loess: Implications for grain size proxy interpretations in Quaternary paleoclimate studies, Earth-Sci Rev, 154, 247-278, 10.1016/j.earscirev.2016.01.006, 2016.
Vandenberghe, J., Renssen, H., van Huissteden, K., Nugteren, G., Konert, M., Lu, H. Y., Dodonov,

A., and Buylaert, J. P.: Penetration of Atlantic westerly winds into Central and East Asia, Quaternary Sci Rev, 25, 2380-2389, 10.1016/j.quascirev.2006.02.017, 2006.
Vandenberghe, J.: Grain size of fine-grained windblown sediment: A powerful proxy for process identification, Earth-Sci Rev, 121, 18-30, 10.1016/j.earscirev.2013.03.001, 2013.
Vandenberghe, J., French, H. M., Gorbunov, A., Marchenko, S., Velichko, A. A., Jin, H., Cui, Z., Zhang, T., and Wan, X.: The Last Permafrost Maximum (LPM) map of the Northern Hemisphere: permafrost extent and mean annual air temperatures, 25–17 ka BP, Boreas, 43, 652-666, 2014.
Varga, G.: Similarities among the Plio-Pleistocene terrestrial aeolian dust deposits in the World and in Hungary, Quatern Int, 234, 98-108, 10.1016/j.quaint.2010.09.011, 2011.
Vriend, M., and Prins, M. A.: Calibration of modelled mixing patterns in loess grain-size distributions: an example from the north-eastern margin of the Tibetan Plateau, China, Sedimentology, 52, 1361-1374, 10.1111/j.1365-3091.2005.00743.x, 2005.
Vriend, M.: Lost in loess: Late Quaternary eolian dust dispersal patterns across Central China inferred from decomposed loess grain-size records, Amsterdam, VU University, The Netherlands, 53 pp., 2007.
Vriend, M., Prins, M. A., Buylaert, J. P., Vandenberghe, J., and Lu, H. Y.: Contrasting dust supply patterns across the north-western Chinese Loess Plateau during the last glacial-interglacial cycle, Quatern Int, 240, 167-180, 10.1016/j.quaint.2010.11.009, 2011.
Wang, H., Mason, J. A., and Balsam, W. L.: The importance of both geological and pedological processes in control of grain size and sedimentation rates in Peoria Loess, Geoderma, 136, 388-400, 10.1016/j.geoderma.2006.04.005, 2006.
Weltje, G. J.: Endmember modeling of compositional data: numerical–statistical algorithms for solving the explicit mixing problem, Journal of Mathematical Geology, 29, 503–549, 1997.
Weltje, G. J., and Prins, M. A.: Genetically meaningful decomposition of grain-size distributions, Sediment Geol, 202, 409-424, 2007.
Wolff, C., Plessen, B., Dudashvilli, A. S., Breitenbach, S. F., Cheng, H., Edwards, L. R., and Strecker, M. R.: Precipitation evolution of Central Asia during the last 5000 years, Holocene, 27, 142-154, 2017.
Xiao, J., Porter, S. C., An, Z. S., Kumai, H., and Yoshikawa, S.: Grain-Size of Quartz as an Indicator of Winter Monsoon Strength on the Loess Plateau of Central China during the Last 130,000-Yr, Quaternary Research, 43, 22-29, DOI 10.1006/qres.1995.1003, 1995.
Yang, F., Zhang, G. L., Yang, F., and Yang, R. M.: Pedogenetic interpretations of particle-size distribution curves for an alpine environment, Geoderma, 282, 9-15, 2016.
Yang, S. L., Ding, F., and Ding, Z. L.: Pleistocene chemical weathering history of Asian arid and semi-arid regions recorded in loess deposits of China and Tajikistan, Geochim Cosmochim Ac, 70, 1695-1709, 10.1016/j.gca.2005.12.012, 2006.
Yang, S. L., and Ding, Z. L.: Advance-retreat history of the East-Asian summer monsoon rainfall belt over northern China during the last two glacial-interglacial cycles, Earth Planet Sc Lett, 274, 499-510, 10.1016/j.epsl.2008.08.001, 2008.
Yang, S. L., and Ding, Z. L.: A 249 kyr stack of eight loess grain size records from northern China documenting millennial-scale climate variability, Geochem Geophy Geosy, 15, 798-814, 10.1002/2013gc005113, 2014.
Ye, W.: Characteristics of physical environment and conditions of loess formation in Yili area, Xinjiang, Arid Land Geography, 22, 9-16 (in Chinese), 1999.

Ye, W., Sang, C., and Zhao, X.: Spatial-temporal distribution of loess and source of dust in Xinjiang, Journal of Desert Research, 23, 514-520 (in Chinese), 2003.
Youn, J. H., Seong, Y. B., Choi, J. H., Abdrakhmatov, K., and Ormukov, C.: Loess deposits in the northern Kyrgyz Tien Shan: Implications for the paleoclimate reconstruction during the Late Quaternary, Catena, 117, 81-93, 10.1016/j.catena.2013.09.007, 2014.
Yu, S. Y., Colman, S. M., and Li, L. X.: BEMMA: A Hierarchical Bayesian End-Member Modeling Analysis of Sediment Grain-Size Distributions, Math Geosci, 48, 723-741, 10.1007/s11004-015-9611-0, 2016.
Zech, R.: A late Pleistocene glacial chronology from the Kitschi-Kurumdu Valley, Tien Shan (Kyrgyzstan), based on Be-10 surface exposure dating, Quaternary Research, 77, 281-288, 10.1016/j.yqres.2011.11.008, 2012.
Zeeden, C., Hambach, U., Veres, D., Fitzsimmons, K., Obreht, I., Bösken, J., and Lehmkuhl, F.: Millennial scale climate oscillations recorded in the Lower Danube loess over the last glacial period, Palaeogeography, Palaeoclimatology, Palaeoecology, (in press), 2016.
Zhang, X. J., Jin, L. Y., Huang, W., and Chen, F. H.: Forcing mechanisms of orbital-scale changes in winter rainfall over northwestern China during the Holocene, Holocene, 26, 549-555, 10.1177/0959683615612569, 2016.
Zhang, X. Y., Arimoto, R., and An, Z. S.: Glacial and interglacial patterns for Asian dust transport, Quaternary Sci Rev, 18, 811-819, 1999.
Zhao, L., Jin, H., Li, C., Cui, Z., Chang, X., Marchenko, S. S., Vandenberghe, J., Zhang, T., Luo, D., and Guo, D.: The extent of permafrost in China during the local Last Glacial Maximum (LLGM), Boreas, 43, 688-698, 2014.
Zhou, L. P., Oldfield, F., Wintle, A. G., Robinson, S. G., and Wang, J. T.: Partly Pedogenic Origin of Magnetic Variations in Chinese Loess, Nature, 346, 737-739, DOI 10.1038/346737a0, 1990.

Fig01

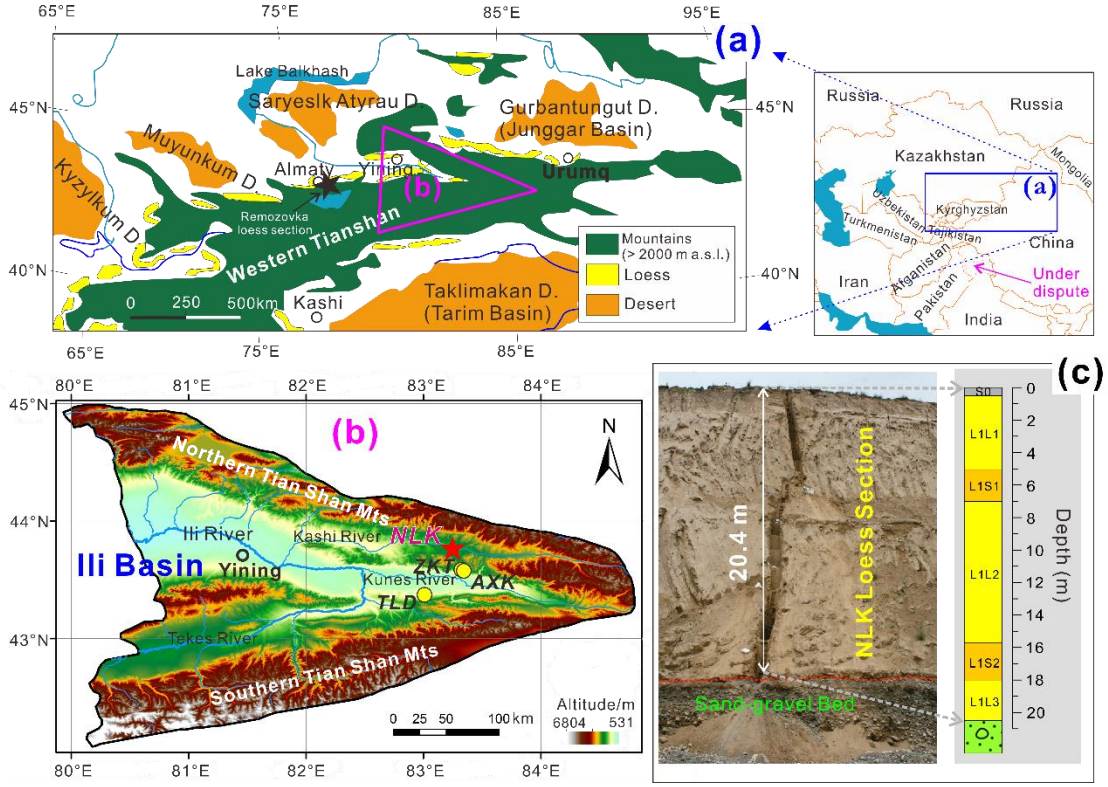
(a)
(b)
(c)
Lake Balkhash
Saryeslk Atyrau D.
Gurbantungut D.
(Junggar Basin)
Muyunkum D.
Kyzylkum D.
Almaty
Yiming
Urumq
Remozovka
loess section
Western Tianshan
Kashi
Taklimakan D.
(Tarim Basin)
Mountains
(> 2000 m a.s.l.)
Loess
Desert
0 250 500km
Russia
Kazakhstan
Mongolia
Kyrghyzstan
Uzbekistan
Turkmenistan
Tajikistan
China
Iran
Afganistan
Pakistan
India
Under
dispute
Northern Tian Shan Mts
Ili River
Kashi River
NLK
Ili Basin
Yining
ZKT
Kunes River
AXK
TLD
Tekes River
Southern Tian Shan Mts
N
0 25 50 100 km
Altitude/m
6804 531
20.4 m
NLK Loess Section
Sand-gravel Bed
S0
L1L1
L1S1
L1L2
L1S2
L1L3
Depth (m)

Fig02

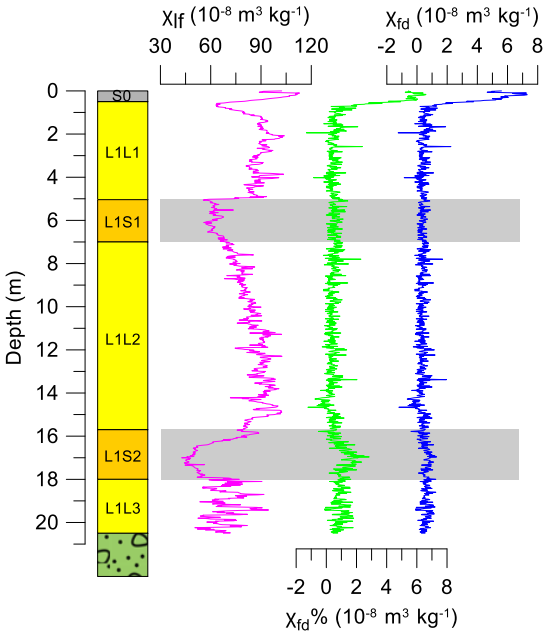
χlf (10-8 m3 kg-1)
30 60 90 120
χfd (10-8 m3 kg-1)
-2 0 2 4 6 8
Depth (m)
0 2 4 6 8 10 12 14 16 18 20
S0
L1L1
L1S1
L1L2
L1S2
L1L3
-2 0 2 4 6 8
χfd% (10-8 m3 kg-1)

Fig03

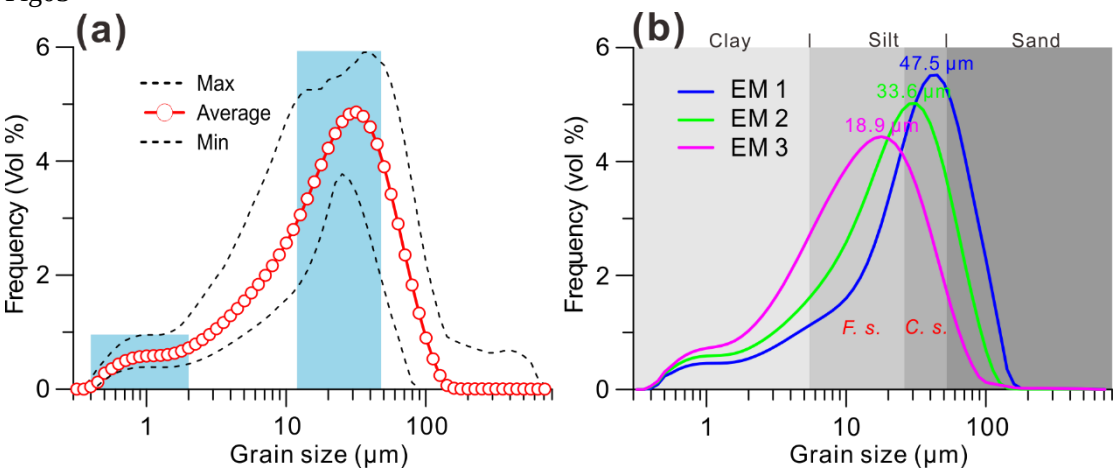
(a)
Max
Average
Min
Frequency (Vol %)
Grain size (μm)
(b)
Clay
Silt
Sand
EM 1
EM 2
EM 3
47.5 μm
33.6 μm
18.9 μm
F. s.
C. s.
Frequency (vol %)
Grain size (μm)

Fig04

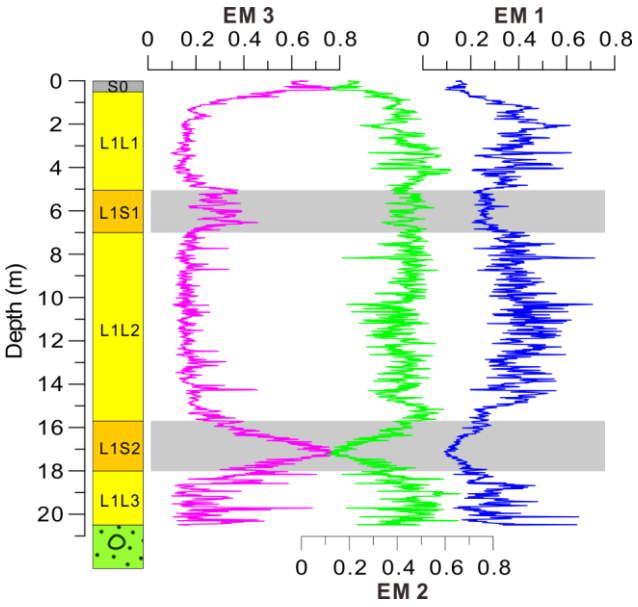
EM 3
0 0.2 0.4 0.6 0.8
EM 1
0 0.2 0.4 0.6 0.8
Depth (m)
0
2
4
6
8
10
12
14
16
18
20
S0
L1L1
L1S1
L1L2
L1S2
L1L3
0 0.2 0.4 0.6 0.8
EM 2

Fig05

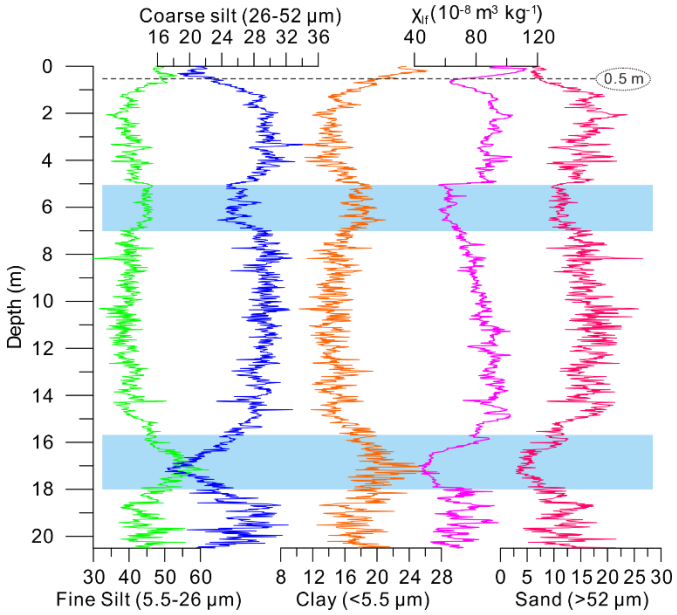
Coarse silt (26-52 μm)
16 20 24 28 32 36
χ_{lf} (10^{-8} m^3 kg^{-1})
40 80 120
0.5 m
Depth (m)
0 2 4 6 8 10 12 14 16 18 20
30 40 50 60
Fine Silt (5.5-26 μm)
8 12 16 20 24 28
Clay (<5.5 μm)
0 5 10 15 20 25 30
Sand (>52 μm)

Fig06

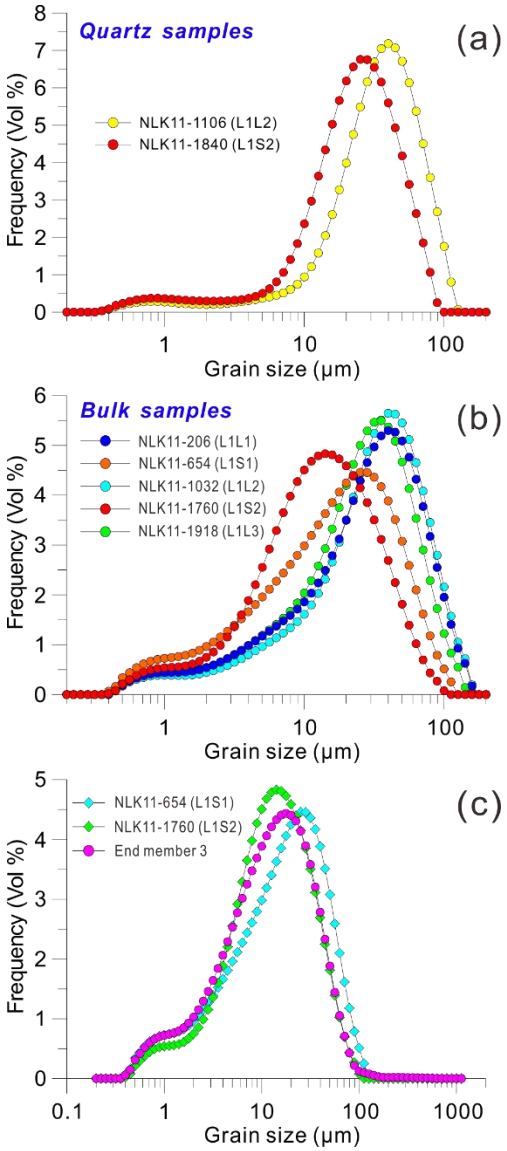
Quartz samples
(a)
NLK11-1106 (L1L2)
NLK11-1840 (L1S2)
Frequency (Vol %)
Grain size (μm)
Bulk samples
(b)
NLK11-206 (L1L1)
NLK11-654 (L1S1)
NLK11-1032 (L1L2)
NLK11-1760 (L1S2)
NLK11-1918 (L1L3)
Frequency (Vol %)
Grain size (μm)
(c)
NLK11-654 (L1S1)
NLK11-1760 (L1S2)
End member 3
Frequency (Vol %)
Grain size (μm)

Fig07

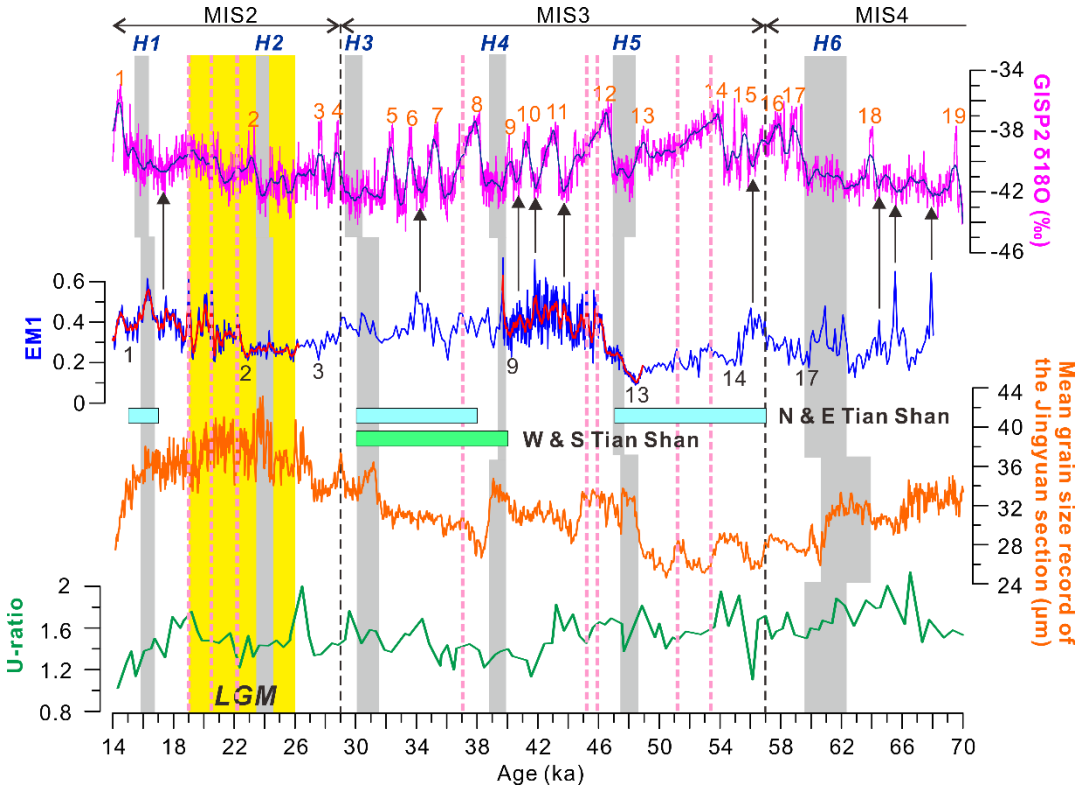
MIS2
MIS3
MIS4
H1
H2
H3
H4
H5
H6
GISP2 δ18O (‰)
-34
-38
-42
-46
EM1
0.6
0.4
0.2
0
N & E Tian Shan
W & S Tian Shan
Mean grain size record of the Jingyuan section (μm)
44
40
36
32
28
24
U-ratio
2
1.6
1.2
0.8
LGM
14
18
22
26
30
34
38
42
46
50
54
58
62
66
70
Age (ka)